Oceanic response to changes in the WAIS and astronomical forcing during the MIS31 superinterglacial

Flavio Justino[1], Douglas Lindemann[1], Fred Kucharski[2], Aaron Wilson[3], David Bromwich[3], and Frode Stordal[4]

[1]Department of Agricultural Engineering, Universidade Federal de Vicosa, PH Rolfs, Vicosa, Brazil
[2]The Abdus Salam International Centre for Theoretical Physics, Trieste, Italy
[3]Polar Meteorology Group, Byrd Polar and Climate Research Center, The Ohio State University, Columbus, OH, USA
[4]University of Oslo,Department of Geosciences, Forskningsparken Gaustadalleen, Oslo, Norway

Correspondence to: Flavio Justino (fjustino@ufv.br)

Abstract. Marine Isotope Stage 31 (MIS31, between 1085 ka and 1055 ka) was characterized by higher extratropical air temperatures and a substantial recession of polar glaciers compared to today. Paleoreconstructions and modeling efforts have increased the understanding of MIS31 interval, but questions remain regarding the role of the Atlantic and Pacific Oceans in modifying climate anomalies associated with the variations in Earth's orbital parameters. Based on multi-century coupled climate simulations, it is shown that under the astronomical configuration of the MIS31 and forced by modified West Antarctic Ice Sheet (WAIS) topography, there exists a substantial increase in the thermohaline flux and its associated northward oceanic heat transport (OHT) in both the Atlantic and Pacific Oceans. In the Atlantic, these changes are driven by enhanced oceanic heat loss to the atmosphere and increased water density. In the Pacific, anomalous wind-driven circulation in concert with stronger meridional overturning circulation results in greater northward OHT that contributes up to 85% of the global OHT anomalies, adding to an overall reduction in sea ice in the Northern Hemisphere (NH) due to Earth's astronomical configuration at the time. Sea-ice changes in the Southern Hemisphere (SH) are highlighted by decreased (increased) cover in Ross (Weddell) Sea.

1 Introduction

As demonstrated by paleoreconstructions and modeling results, interglacial stages such as the MIS5e, MIS15, and MIS31 show large similarities to predicted future Earth climate with regards to global sea-level changes, temperature, and ice-sheet distributions (Lisiecki and Raymo (2005); Maiorano et al. (2009); Coletti et al. (2014); Yin and Berger (2012); Melles et al. (2012); Stocker et al. (2013)). However, many issues are still required to be fully addressed concerning the nature of long-term ocean dynamics. In particular, the climate response to potential changes in the Meridional Overturning Circulation (MOC) and the OHT are of concern. Moreover, paleoreconstructions and modeling results disagree with respect to the North Hemisphere warming during the MIS31, suggesting the need for a better understanding of this interglacial and other warmer climates (Coletti et al. (2014); Melles et al. (2012)) as well.

At large, these differences arise from limited constrained paleoreconstructions with improper climate model boundary conditions, which are crucial for assuring the statistical climate equilibrium that may be modified during interglacial climates (Yin

(2013)). Modeling interglacial stages requires changes in internal and external forcing involving modifications of the ice sheet topography (Pollard and DeConto (2009); Melles et al. (2012)), atmospheric CO_2 concentration (Honisch et al. (2009)), and the planetary astronomical configuration (Erb et al. (2015); Yin (2013)).

To gain insight on the matter, analyses have focused on the climate response to these individual drivers (Knorr and Lohmann (2014); Yin and Berger (2012); Pollard and DeConto (2009)). Among other effects, insolation plays a dominant role in defining high-northern latitude temperature and sea ice (Yin and Berger (2012)). The longitude of the perihelion (precession) is also found to lead changes in the equatorial Pacific seasonal cycle (Erb et al. (2015). Meanwhile, past fluctuations in atmospheric CO_2 concentration have been claimed to induce long-term surface and deep-water temperature trends (Knorr and Lohmann (2014)). The global climate response to these forcings is governed by a complex interaction relying on processes not only occurring at the air-sea interface but also in sub-surface layers where a substantial amount of heat is stored (Meehl et al. (2011); Yin and Berger (2012)). Past (Ford et al. (2015)) and current (Philander et al. (1989)) climates have also experienced ripple effects worldwide related to deviations from the equatorial oceanic mean state and seasonal cycle. Indeed, increased OHT from the Pacific into the Arctic associated with changes in Antarctic ice volume has been argued to affect the Beringian climate during interglacial epochs (Coletti et al. (2014)).

Accordingly, this study aims to disentangle the individual contributions of the WAIS and the astronomical configuration during the MIS31 climate. Mechanisms related to the combined effects of these forcing and associated with the inter-hemispheric coupling, including the potential role of the OHT, wind-driven and thermohaline changes, as regulator of the MIS31 anomalous climate are explored. Oceanic dynamical changes during interglacial intervals are crucial for determining the large-scale atmospheric circulation and temperature distribution (Coletti et al. (2014)). Answers to these questions are pursued by employing the International Centre for Theoretical Physics - Coupled Global Climate Model (ICTP-CGCM) (Kucharski et al. (2015)). The astronomical forcing is assumed to represent 1072 ka based on the warmest summer month in lake El'gygytgyn reconstruction (Coletti et al. (2014); Melles et al. (2012)). Results provide insight on the air-sea exchange processes and large-scale ocean dynamics characteristic of this epoch.

2 Coupled model and experimental design

The ICTP-CGCM control simulation (CTR) is run under present day orbital forcing for over 2000 years since proper evaluations of long-term ocean-atmosphere processes require statistical equilibrium representation of the climate state, particularly for paleoclimatic features in a coupled atmosphere-ocean model (Peltier and Solheim (2004)).

The CO_2 concentration in our CTR climate is 325 ppm, because it allows for a better comparison with the reconstructed value in the MIS31 interval. Additionally, 325 ppm characterizes 1950 and is not strongly influenced by the recent temperature and CO_2 upward trend.

The ICTP-CGCM, consisting of the atmospheric global climate model "SPEEDY" version 41 (Kucharski et al. (2006)) coupled to the Nucleus for European Modelling of the Ocean (NEMO) model (Madec (2008)) with the OASIS3 coupler (Valcke (2013)), is used in this study. The atmospheric component runs at T30 horizontal resolution and there are eight levels in

the vertical. The model includes physically-based parameterizations of large-scale condensation, shallow and deep convection, shortwave and longwave radiation, surface fluxes of momentum, heat and moisture, and vertical diffusion. NEMO is a primitive equation z-level ocean model based on the hydrostatic and Boussinesq approximations. This version applies a horizontal resolution of 2° and a tropical refinement to 0.5°. The ocean component has 31 vertical levels with layer thicknesses ranging from 10 m at the surface to 500 m at the ocean bottom (16 levels in the upper 200 m). Additional details of the ICTP-CGCM are described by Justino et al. (2015) and Kucharski et al. (2015).

2.1 Model performance of the CTR climate

To evaluate the reliability of the coupled model to represent the present day climate (control run), Fig. 1 shows SST differences between the CTR run and the NOAA Optimum Interpolation (OI) Sea Surface Temperature V2 (NOAA-OI-SST-V2) (Reynolds et al. (2002)) and sea-ice extent based on the Hadley Centre Sea Ice and Sea Surface Temperature data set (HadISST) (Rayner et al. (2003)). The modeled evaporation minus precipitation (E - P) flux is compared to the Interim Reanalysis from the European Centre for Medium-Range Weather Forecasts (ECMWF) ERA-Interim (ERAI) (Dee et al. (2011)). It has to be mentioned that Kucharski et al. (2015) has provided detailed analyses of the present day climate simulated by the ICTP-CGCM.

Comparison between the ICTP-CGCM and NOAA-OI-SST-V2/HadISST for the annual SST pattern and sea-ice extent (Fig. 1a), shows differences in the extratropical ocean where the ICTP-CGCM is colder than NOAA-OI-SST-V2 due to differences in the atmospheric flow. However, it should be stressed that overall SST differences are in the range of $\pm\,2°C$.

Evaluation of the sea-ice cover and margin (yellow line in Fig. 1b) also shows that the model compares well with HadISST insofar as annual mean conditions are concerned, with only reduced sea-ice extent in the South Atlantic (Fig. 1b). Analysis of E - P flux demonstrates that our coupled model is able to reasonably reproduce the main characteristics of the ERAI E - P flux (Fig. 1c), but the zonal averages reveal that the ICTP-CGCM is wetter than the ERAI in the equatorial belt and SH mid-latitudes (not shown). However, differences are less than 1 mm day^{-1}.

The E - P flux associated with the Intertropical Convergence Zone (ITCZ) demonstrates that similar to other CGCMs (Jia-Jin (2007)), improvements are still necessary in order to better reproduce equatorial climate dynamics including decreased precipitation in the Pacific Warm Pool and over the southern part of the South Atlantic. Thus, the ICTP-CGCM is able to satisfactorily reproduce the basic climate features at relatively low computational cost. For instance, 100 model years could be achieved in 2 days with 16 processors. Therefore, the sensitivity of a particular process or sub-component of the climate system across a wide range of parameters can be investigated.

Design of the sensitive experiments

To evaluate the climate impact of changes in the WAIS topography and the astronomical forcing during the MIS31 interglacial, 3 additional sensitivity experiments have been conducted for 1000 years (Table 1 supp. material):

1. TOPO - applies the WAIS topography as proposed by previous studies (Pollard and DeConto (2009); Justino et al. (2015));

2. AST - conducted with astronomical configuration characteristic of the 1072 ka (Berger (1978); Coletti et al. (2014));

3. MIS31 - the combined effect of the forcing described in TOPO and AST.

In all sensitivity experiments, the CO_2 concentration is set to 325 ppm. For the MIS31 interval this is reasonable based on boron isotopes in planktonic foraminifera shells Honisch et al. (2009). Though the Greenland Ice Sheet (GIS) may have been reduced as compared to present day (Melles et al. (2012)), it has been shown that a deglaciated Greenland does not play a substantial role in driving NH temperatures during the MIS31 (Coletti et al. (2014)). Therefore, the GIS in ICTP-CGCM reflects present day conditions.

Our simulation does not include changes in oceanic gateways, because there is no conclusive global land-sea mask reconstruction for the MIS31 interval. The WAIS topography has been modified, but no changes in sea level have been applied in our modeling experiment. However, the modified WAIS reflects sea water albedo in the sensitivity runs.

3 Climate response to MIS31 forcing

The WAIS collapse

Previous work (Justino et al. (2015)) using a simplified low resolution ocean model ($3° \times 3°$) has shown that the incorporation of a modified WAIS topography characteristic of the MIS31 interval, results in generally warmer global surface temperatures with enhanced positive anomalies between 50-70°S. It should be noted that the warming delivered by the ICTP-CGCM TOPO simulation is substantially smaller as compared to previously found (Justino et al. (2015)) (Fig. 2a). Lower surface temperature anomalies noted in the Ross and Weddell Seas only extend out to 40°S.

There are several factors related to differences in global temperature anomalies between these two studies. Stronger air-sea heat flux exchanges and a more realistic atmosphere-ocean interface are present in the ICTP-CGM. In fact, the previous model results show much weaker SH westerly flow leading to warmer SSTs across the high latitudes of the SH compared to the present study (not shown). The previous study also reflects weaker teleconnections between the tropical and extratropical regions related to the El Nino-Southern Oscillation (ENSO) (Severijns and Hazeleger (2010)). NEMO (present model) and CLIO (previous model) are characterized by drastically modified ENSO related-tropical variability in terms of variance and magnitude (Severijns and Hazeleger (2010); Park et al. (2009)). The NEMO ocean model used in the present study can properly simulate the global oceanic features as it resolves convective and mesoscale processes in the mixed layer and themocline related to the ENSO.

It has long been recognized that the effect of the air-sea coupling by the Ekman layer for the surface climate is remarkable. For instance, CGCMs driven by a lower resolution oceanic component are very limited in their ability to reproduce the wind-driven upwelling, and therefore are warmer than those models running with higher resolution. More importantly, low resolution ocean-atmosphere models struggle to reproduce the OHT. In this line, it has to be mentioned that SPEEDO simulates weaker

Atlantic Overturning Circulation (NADW = 8 Sv), and therefore allows for larger storage of heat in the Southern Hemisphere due to orth Hemisphere heat piracy assumption. The NADW in the ICTP-CGCM matches observations (22 Sv) closely.

Under present-day conditions, katabatic winds flowing offshore from the continent over the Weddell Sea are responsible for maintaining cold air over the sea-ice edge. Modeled Weddell Sea warming in the TOPO simulation is related to weaker katabatic winds and reduced continental cold air advection Justino et al. (2015) due to a collapsed WAIS. It should be noted that over sea-ice covered region (Fig. 2), temperatures reflect sea-ice temperatures and not SST. Reduced sea-ice thickness and increased exchange of heat by the underlying ocean also enhances the anomalous warming pattern in this region. Higher temperatures in the Ross Sea in TOPO is supported by the Ocean Drilling Program (ODP) site 1165 and by the marine glacial record of the AND-1B sediment core in the Ross Ice Shelf (Naish et al. (2009)).

The AST forcing

Turning to the impact of astronomical changes on global surface temperatures (AST minus CTR), warming is evident in the northeastern Pacific and Atlantic Oceans (Fig. 2b). The orbital elements during the MIS31 interval are characterized as high obliquity and eccentricity with enhanced boreal summer insolation. Downward solar radiation differences at the top of the atmosphere between AST and CTR reach values of up to 50 W m^{-2} at 60°N (not shown). These seasonal changes project onto annual conditions due to the remnant insolation effect (Yin and Berger (2012)). In fact, increased heat in the oceanic surface layer during the summer months hinders the winter cooling which over extratropical latitudes hampers the increase in sea-ice cover. Thus, vigorous oceanic heat exchange leads to higher near-surface air temperatures compared to the CTR run.

The NH (SH) warming (cooling) is primarily associated with intensified (weakened) summer insolation that is dominant in the polar and subtropical regions. In addition to reduced insolation in the SH, stronger southeast trade winds and westerlies (Fig. 2d) lead to lower surface temperatures related to stronger equatorial upwelling and modified Ekman dynamics (McCreary and Lu (1194)). The wind-evaporation-SST feedback also plays a role due to modification in the latent heat through evaporation (Wang et al. (1999)).

Elsewhere, the atmospheric circulation and the heat exchanges due to air-sea interactions play prominent roles in defining annual mean conditions. The incorporation of the astronomical forcing also delivers anomalous surface temperature patterns in such a way that the Atlantic Ocean anomalies resemble present-day conditions under the positive phase of the Atlantic Multicultural Oscillation (AMO) (Delworth and Mann (2000)). Surface temperature anomalies in the North Pacific on the other hand, depict the warm phase of the Pacific Decadal Oscillation (Zhang et al. (1997)).

Surface climate response to joined AST and WAIS forcing

It has to be noted that a comparison between the MIS31 and the AST runs (see supplementary material, Fig. 1c) can be used to identify in more detail the effect of the WAIS topography during the MIS31 climate. Differences between MIS31 and AST

demonstrate that the substantial reduction of sea-ice cover and warmer surface in the former over the Ross and in some extent over Weddell Seas is substantially affected by the reduction of the WAIS (Supplementary Fig. 1c).

The surface temperature patterns in the NH are associated with stronger mid-latitude and polar westerlies over the Kuroshio/Oyashio region but weaker northeast trade winds over the central-eastern Pacific with further implications for the OHT. Indeed, weaker

5 surface winds account for the eastern Pacific warming (Fig. 2d) due to both reduced Ekman drift and reduced evaporative cooling. Results from the ODP Sites 806 and 849 (McClymont and Rosell-Melé (2005)) also support changes in the zonal circulation in the equatorial Pacific. Figure 2c shows that in general, the MIS31 modeled surface temperatures and reconstructions (red dots) (Scherer et al. (2008); Voelker et al. (2015); McClymont and Rosell-Melé (2005); Naish et al. (2009)) show good agreement but should be evaluated with care in the western equatorial Pacific. Proper results (blue squares) (Becquey and Gersonde

10 (2002); Teitler et al. (2015); Villa et al. (2008)) are also located in the sub-Antarctic south Atlantic and Prydz Bay area.

Changes in surface temperature and winds have the potential to generate sea-ice anomalies (Table 1, Fig. 2). Modification of the WAIS topography is associated with changes in sea-ice area and volume particularly in the Atlantic Ocean. Changes in the astronomical forcing on the other hand are responsible for climate anomalies in a global perspective. These results cast uncertainty on previous studies based on in situ reconstructions that assume overall warming and sea-ice free conditions in the

15 Southern Ocean as compared to the present-day climate (Scherer et al. (2008)).

The sensitivity experiments demonstrate that warmer surface temperatures and reduced sea ice are only simulated in the Ross Sea region, in agreement with the Cape Roberts Project-1 results and data from the Antarctic Geological Drilling project (ANDRILL) (Naish et al. (2009)) (Fig. 2). In fact, outside of the Ross Sea, Antarctic sea ice during the MIS31 interval should have been more abundant compared to current conditions. In the NH, sea-ice cover is substantially reduced by up to 85% (25%)

20 in volume (area) in the AST and MIS31 runs. Recall however, that the ICTP-CGM boundary conditions represent the 1072 ka maximum warming period and not the entire MIS31 epoch that extends through 1.08 and 1.05 Ma.

The global climate response due to combined effect of changing WAIS topography and astronomical forcing (MIS31 simulation)) is primarily the result of changes in the latter forcing, as Fig. 2c shows a similar surface temperature anomaly pattern as Fig. 2b. Nevertheless, the combined forcing appear to be a linear sum of both in the vicinity of Antarctica (Supplementary Fig.

25 1c). Intensified warming is shown in the Ross Sea (the result of warmer surface temperatures in TOPO and AST) but reduced cooling in the Weddell Sea, where the absence of the WAIS topography in the joint effect reduces the strong cooling associated with changes in the astronomical forcing.

NH sea ice negligibly changes due to the collapse of WAIS topography as only a small increase in sea-ice cover occurs (Table 1). WAIS topography plays a greater role in defining anomalies in the Weddell and Ross Seas. This is revealed by differences

30 between the MIS31 and AST experiments (supplementary material). The MIS31 simulation is warmer in the Weddell and Ross Seas by up to 1.5°C with respect to AST, which is accompanied by reduce sea-ice cover by about 10%.

Further comparisons between modeled results and paleoreconstructions of the northern Pacific-Asian region Melles et al. (2012); Coletti et al. (2014) show good agreement insofar as warmer conditions are concerned. For instance, in the North Atlantic, warmer surface temperatures in Fig. 2 also match reconstructions of surface temperatures from Site U1387 near

35 southern Portugal Voelker et al. (2015). However, there are regional discrepancies between model results in this study and

reconstructions. While reduced sea ice and warmer surface temperatures in the Ross sea region are supported, disagreement is found in the southern Atlantic (e.g ODP sites 1090 Becquey and Gersonde (2002) and Prydz Bay Villa et al. (2008) areas).

Changes in MOC and OHT

Changes in atmospheric circulation, surface temperatures, and sea ice modify the MOC. There is particular interest in evaluating changes to the MOC associated with warming and/or freshening of the NH high-latitude surface waters due to natural variability (as shown here), and/or including anthropogenic induced-global warming. The Atlantic MOC is a key element of the climate system, because it carries a substantial amount of heat poleward, and on long timescales, plays an important role in coupling the SH and NH (Broecker (1998)).

Figure 3a,d shows that the ICTP-CGCM properly reproduces the magnitude of the North Atlantic Deep Water (NADW, 20 Sv) compared to data-based estimates (Talley et al. (2003)). Analysis of the density contribution in the main sites of the NADW formation demonstrate that thermal changes dominate. Indeed, stronger extratropical winds increase the vertical air-sea temperature contrast and consequently the ocean-atmosphere heat exchange (Schmitt et al. (1989); Speer and Tziperman (1992)). This leads to stronger convective mixing especially in the North Atlantic (Fig. 3a). The CTR shows two regions of density gain (Fig. 3a): the western North Atlantic and the Nordic Sea, where cold and dry air masses blow over relatively warm water.

The modification of the WAIS leads to slightly reduced rate of formation of the NADW and a shallower cell as compared to the CTR (Fig. 3b,d). This was not anticipated, as Table 1 shows slightly increased sea ice associated with brine rejection, and potentially with small increases in the density of sea water in the TOPO simulation. However, changes in surface salinity dominate water density anomalies only over sea-ice margins (Speer and Tziperman (1992)). The weakening of the NADW in the TOPO simulations is associated with reduced heat exchange between the ocean and the atmosphere in the Labrador and Greenland, Iceland, Norwegian (GIN) Seas due to increased sea ice, thereby reducing convective mixing (Fig. 3b).

This is also demonstrated by the surface density anomalies, a combination of the thermal and haline density contributions (Speer and Tziperman (1992); Justino et al. (2014)) (Fig. 3b). It can also be argued that intensified intrusion of Antarctic water between 3000-4000 m in the North Atlantic results in increased vertical oceanic stability/stratification, hampering oceanic convection. Similar results have been reported for Last Glacial Maximum conditions where colder conditions in the North Atlantic led to a weaker NADW flow (McManus et al. (2004); Peltier and Solheim (2004)).

Turning to the AST and MIS31 experiments, Fig. 3 shows that despite reduced sea ice, there are thermally-increased surface water density anomalies in the main sites of deep water formation, particularly in the Labrador and GIN seas (Fig. 3c,f). Thus, the NADW in these experiments is deeper and intensified compared to the control simulation (Fig. 3f). Intensified MOC and its associated OHT have also been claimed to prevent NH cooling during the MIS11 interval (Dickson et al. (2009)).

As shown by the thermal contribution, increases in the MOC (Fig. 3f) are related to intensified westerly atmospheric flow in the northern North Atlantic (Fig. 2d), leading to strong convective mixing. It can also be argued that less intrusion of the Antarctic water in the North Atlantic above 4000 m results in vertical instability favoring oceanic convection (Haupt and Seidov

(2012)). Moreover, northward mass transport between 0-1000 m in the NH mid-latitudes is enhanced in the AST and MIS31 simulations compared to the CTR (Fig. 3f). An intensified MOC during the MIS31 has also been suggested using paleoreconstructions (Scherer et al. (2008)).

Changes in atmospheric and oceanic features, such as those discussed above, also produce modifications in OHT (Fig. 4a).

5 The OHT in the Atlantic is mainly driven by the MOC cell, while in the Pacific it is driven by the horizontal wind-driven circulation (Ferrari and Ferreira (2011)). The OHT in the TOPO changes slightly compared to the CTR. However, in the AST and MIS31 simulations, a clear pattern of increased astronomically-driven northward OHT is present (Fig. 4a).

As expected, enhanced OHT in the Atlantic Ocean in the AST and MIS31 simulations is related to stronger MOC (Fig. 3f) and to some extent, to the changes in the wind-driven circulation.

10 In mid-latitudes, intensified atmospheric westerly flow (Fig. 2d) in the vicinity of the American continent is simulated in the AST and MIS31 experiments, which contribute to the enhanced OHT via the transport of warmer subtropical water to mid-latitudes (Fig. 4a).

Figure 3f also shows a weakening of the southward flow in the upper ocean levels (0-900 m), which indicates that most water is transported in intermediated levels below 1000 m which includes the NADW contribution.

15 Interestingly, Fig. 4a also shows the dominant contribution from the Indian-Pacific sector to global OHT anomalies. This finding is in line with previous results demonstrating that a prescribed enhancement of OHT into the Arctic Ocean results in better correspondence between modeling results and the Lake El'gygytgyn reconstruction (Coletti et al. (2014)). Enhanced OHT during the MIS31 is also supported by the ODP site 806 and 849 (McClymont and Rosell-Melé (2005)).

The present day OHT in the Pacific sector is associated with the subtropical wind-driven circulation in the western Pacific

20 (Kleeman et al. (1999)); however, under MIS31/AST conditions, important contribution may also arises from density changes. The wind-driven part may be assessed by computing the Sverdrup transport (Eq. 1), defined as:

$$\psi(x) = \frac{1}{\beta\rho} \int\limits_{x_e}^{x} \frac{\partial \tau_x}{\partial y} dx \qquad (1)$$

where β is the meridional derivative of the Coriolis parameter, ρ is the mean density of sea water, and τ_x is the zonal component of the wind stress. The integral is computed from the eastern to the western boundary in the North Pacific using

25 modeled atmospheric wind stress data. The ICTP-CGCM model simulates the Sverdrup transport quite well (not shown) compared to the magnitude of the Sverdrup transport estimated from the International Comprehensive Ocean-Atmosphere Data Set (ICOADS) (Woodruff et al. (2011)). However, the front that separates the subtropical and the polar gyre is shifted northward in the ICTP-CGCM compared to the ICOADS data.

The Sverdrup transport anomalies between the MIS31 and control experiments (Fig. 4b) show an overall strengthening by up

30 to 20% of the mass transport between 25°N-45°N, as a result of enhanced wind stress curl. This in turn decreases the amount of warmer water reaching the North Pacific (see SST anomalies) and modifies the OHT, as discussed below.

The density contribution (Fig. 3a,b,c) shows that the incorporation of the astronomical forcing in the AST/MIS31 experiments led to potential increases in water density in the North Pacific. The initial speed up of the subtropical gyre associated with

modified mid-latitude westerlies, and the associated heat loss from the ocean to the atmosphere northward of 40°N dominates the surface density. Subsequently, this leads to the formation of the Pacific Meridional Overturning Circulation (PMOC).

Reduction in sea-ice cover reduces the density changes in the sea-ice/water interface, but this contribution to the PMOC weakening is marginal and confined to the Arctic region. Additional contribution to the PMOC is provided by increased evaporation in AST/MIS31 runs compared to the precipitation anomalies, which further increase the surface salinity in the North Pacific (Fig. 4d). Figure 5 summarizes the air-sea interaction mechanisms which are involved in the PMOC formation rate.

Evaluation the individual contributions of the wind-driven and thermohaline circulation to North Pacific OHT across 26°N shows that under CTR conditions from surface to 300 m depth, the wind-driven component contributes up to 58% (0.55 PW) of the total OHT (not shown). These values are similar to previous estimates based on observations (Talley (2003)) showing that in subtropics and mid-latitudes, most of the OHT is due to the North Pacific gyre. An additional 42% (0.40 PW) of OHT occurs in the 300-1200 m layer.

For the MIS31 climate, the OHT associated with the wind-driven circulation (0-300 m) at 26°N is less than during CTR and represents 44% of the total (55% in the CTR). This indicates that at this latitude important contribution to OHT is related to the thermohaline circulation (Fig. 4c), below the Ekman layer. In comparison to the CTR simulation, this represents an increase of 16%, from 40% in the CTR to 56% in the MIS31. It should to be mentioned however, that separating the thermohaline and wind-driven contributions should be interpreted carefully, as the wind-driven density transport partly drives the thermohaline circulation (Talley (2003)).

As shown by vertically integrating the zonal and meridional OHT at basin scale, the contribution of the gyre circulation is dominant in particular between 30-45°N (Supplementary Figs. 2a,c). Under MIS31 conditions, zonally induced OHT is even stronger (Supplementary Fig. 2b), but northward of 45°N the role of the meridional contribution should be taken into account (Supplementary Fig. 2d). Hence, the evaluation of the OHT in a single longitudinal belt does not fully describe the OHT picture insofar as characteristics of large scale domains are needed.

The enhanced northern Pacific OHT certainly contributes to reduced sea-ice cover in the Arctic, but the major driver is the astronomical forcing. Although theoretically is not possible to separate these effects (oceanic and astronomical influences) as the former is caused by the latter, sea-ice changes in the portion of the Russian Arctic (Fig. 2 in the supp. mat.) are larger than in the Western Hemisphere/Nordic Seas, where sea-ice is more affected by the North Atlantic heat transport (Knutti et al. (2004)).

4 Concluding Remarks

Despite limitations associated with the atmospheric model component employed in this study (only 8 vertical levels), the findings reasonably match paleoreconstructions in the framework of the Ocean Drilling Program, ANDRILL, and other individual proxy data (Fig. 2c). These modeling results have enormous implications for paleoreconstructions of the MIS31 climate that assume overall ice free conditions in the vicinity of the Antarctic continent. Since these reconstructions may depict dominant

signals in a particular time interval and locale, they cannot be assumed to geographically represent large-scale domains and their ability to reproduce long-term environmental conditions should be considered with care. Finally, it is important to emphasize that understanding past interglacial intervals that are characterized by a depleted WAIS can shed light on the potential effects of increasing atmospheric CO_2, as the stability of the WAIS will be a key climate factor in decades to come.

Author contributions. F. Justino designed the study, wrote large portions of the manuscript and performed, data processing and plotting. D. Lindemann and F. Kucharski performed all model simulations. All authors substantially contributed to interpretation of the results.

Competing interests. The authors declare that they have no competing financial interests.

Acknowledgements. This work was supported by the the Brazilian National Research Council projects 232718/2014-8 and 407681/2013-2.
5 The first author also thank the Byrd Polar and Climate Research Center for providing the necessary infrastructure.

. NOAA-OI-surface temperature-V2 and ICOADS data are provided by the NOAA/OAR/ESRL PSD, Boulder, Colorado, USA, from their Web site at http://www.esrl.noaa.gov/psd/. ERAI E - P flux was provided by the National Center for Atmospheric Research Staff (Eds),"The Climate Data Guide: ERA-Interim: derived components.", retrieved from https://climatedataguide.ucar.edu/climate-data/era-interim-derived-components, last modified 02 Jan 2014.

References

Becquey, S. and Gersonde, R.: Past hydrographic and climatic changes in the Subantarctic Zone of the South Atlantic - The Pleistocene record from ODP Site 1090, Palaeogeography, Palaeoclimatology, Palaeoecology, 182, 221 – 239, doi:http://dx.doi.org/10.1016/S0031-0182(01)00497-7, http://www.sciencedirect.com/science/article/pii/S0031018201004977, 2002.

5 Berger, A.: Long-term variations of daily insolation and Quaternary climatic changes, Journal of the Atmospheric Sciences, 35, 2362–2367, doi:http://dx.doi.org/10.1175/1520-0469(1978)035<2362:LTVODI>2.0.CO;2, 1978.

Broecker, W.: Paleocean circulation during the last deglaciation. A bipolar seesaw?, Paleoceanography, 13, 119–121, 1998.

Coletti, A. J., DeConto, R. M., Brigham-Grette, J., and Melles, M.: A GCM comparison of Plio-Pleistocene interglacial-glacial periods in relation to Lake El'gygytgyn, NE Arctic Russia, Climate of the Past Discussions, 10, 3127–3161, doi:10.5194/cpd-10-3127-2014,

10 http://www.clim-past-discuss.net/10/3127/2014/, 2014.

Dee, D. P., Uppala, S. M., Simmons, A. J., Berrisford, P., Poli, P., Kobayashi, S., Andrae, U., Balmaseda, M. A., Balsamo, G., Bauer, P., Bechtold, P., Beljaars, A. C. M., van de Berg, L., Bidlot, J., Bormann, N., Delsol, C., Dragani, R., Fuentes, M., Geer, A. J., Haimberger, L., Healy, S. B., Hersbach, H., Hólm, E. V., Isaksen, L., Kallberg, P., Ki ohler, M., Matricardi, M., McNally, A. P., Monge-Sanz, B. M., Morcrette, J.-J., Park, B.-K., Peubey, C., de Rosnay, P., Tavolato, C., Thépaut, J.-N., and Vitart, F.: The ERA-Interim reanalysis:

15 configuration and performance of the data assimilation system, Quarterly Journal of the Royal Meteorological Society, 137, 553–597, doi:10.1002/qj.828, http://dx.doi.org/10.1002/qj.828, 2011.

Delworth, T. L. and Mann, M. E.: Observed and simulated multidecadal variability in the Northern Hemisphere, Climate Dynamics, 16, 661–676, doi:10.1007/s003820000075, http://dx.doi.org/10.1007/s003820000075, 2000.

Dickson, A. J., Beer, C. J., Dempsey, C., Maslin, M. A., Bendle, J. A., McClymont, E. L., and Pancost, R. D.: Oceanic forcing of the Marine

20 Isotope Stage 11 interglacial, Nature Geoscience, 2, 428–433, doi:doi:10.1038/ngeo527, 2009.

Erb, M., Broccoli, A., Graham, N., Clement, A., Wittenberg, A., and Vecchi, G.: Response of the equatorial pacific seasonal cycle to orbital forcing, Journal of Climate, 28, 9258–9276, doi:10.1175/JCLI-D-15-0242.1, 2015.

Ferrari, R. and Ferreira, D.: What processes drive the ocean heat transport?, Ocean Modelling, 38, 171 – 186, doi:http://dx.doi.org/10.1016/j.ocemod.2011.02.013, http://www.sciencedirect.com/science/article/pii/S1463500311000485, 2011.

25 Ford, H. L., Ravelo, A. C., and Polissar, P. J.: Reduced El Nino-Southern Oscillation during the Last Glacial Maximum, Science, 347, 255–258, doi:10.1126/science.1258437, 2015.

Haupt, B. and Seidov, D.: Modeling geologically abrupt climate changes in the Miocene: Potential effects of high-latitudinal salinity changes, Natural Science, 4, 149–158, doi:10.4236/ns.2012.43022, 2012.

Honisch, B., Hemming, N. G., Archer, D., Siddall, M., and McManus, J. F.: Atmospheric Carbon Diox-

30 ide Concentration Across the Mid-Pleistocene Transition, Science, 324, 1551–1554, doi:10.1126/science.1171477, http://www.sciencemag.org/content/324/5934/1551.abstract, 2009.

Jia-Jin, L.: The double-itcz problem in ipcc ar4 coupled gcms: ocean-atmosphere feedback analysis, Journal of Climate, 20, 4497–4525, doi:http://dx.doi.org/10.1175/JCLI4272.1, 2007.

Justino, F., Marengo, J., Kucharski, F., Stordal, F., Machado, J., and Rodrigues, M.: Influence of Antarctic ice sheet lowering on the Southern

35 Hemisphere climate: modeling experiments mimicking the mid-Miocene, Climate Dynamics, pp. 1–16, doi:10.1007/s00382-013-1689-9, http://dx.doi.org/10.1007/s00382-013-1689-9, 2014.

Justino, F., Silva, A. S., Pereira, M. P., Stordal, F., Lindemann, D., and Kucharski, F.: The Large-Scale Climate in Response to the Retreat of the West Antarctic Ice Sheet, J. Climate, doi: http://dx.doi.org/10.1175/JCLI-D-14-00284.1, 2015.

Kleeman, R., McCreary, J. P., and Klinger, B. A.: A mechanism for generating ENSO decadal variability, Geophysical Research Letters, 26, 1743–1746, doi:10.1029/1999GL900352, http://dx.doi.org/10.1029/1999GL900352, 1999.

5   Knorr, G. and Lohmann, G.: Climate warming during Antarctic ice sheet expansion at the Middle Miocene transition, Nature Geoscience, 7, 376–381, doi:10.1038/ngeo2119, 2014.

Knutti, R., Flueckiger, J., Stocker, T., and Timmermann, A.: Strong hemispheric coupling of glacial climate through continental freshwater discharge and ocean circulation, Nature, 430, 851–856, 2004.

Kucharski, F., Molteni, F., and Bracco, A.: Decadal interactions between the western tropical Pacific and the North Atlantic Oscillation,

10   Clim. Dyn., 26, 79–91, 2006.

Kucharski, F., Ikram, F., Molteni, F., Farneti, R., Kang, I., No, H., King, M., Giuliani, G., and Mogensen, K.: Atlantic forcing of Pacific decadal variability, Climate Dynamics, 7, 1169–1188, doi:inpress, http://www.clim-past.net/7/1169/2011/, 2015.

Lisiecki, L. E. and Raymo, M. E.: A Pliocene-Pleistocene stack of 57 globally distributed benthic δ^{18}O records, Paleoceanography, 20, n/a–n/a, doi:10.1029/2004PA001071, http://dx.doi.org/10.1029/2004PA001071, pA1003, 2005.

15   Madec, G.: NEMO: the OPA ocean engine, Note du Pole de Modelisation, pp. 1–110, Note du Pôle de modélisation de l'Institut Pierre-Simon Laplace No 27, http://dx.doi.org/10.1029/137GM07, 2008.

Maiorano, P., Marino, M., and Flores, J.-A.: The warm interglacial Marine Isotope Stage 31: Evidences from the calcareous nannofossil assemblages at Site 1090 (Southern Ocean), Marine Micropaleontology, 71, 166 – 175, doi:http://dx.doi.org/10.1016/j.marmicro.2009.03.002, http://www.sciencedirect.com/science/article/pii/S0377839809000255, 2009.

20   McClymont, E. L. and Rosell-Melé, A.: Links between the onset of modern Walker circulation and the mid-Pleistocene climate transition, Geology, 33, 389–392, 2005.

McCreary, J. and Lu, P.: Interaction between the subtropical and the equatorial ocean circulations: The subtropical cell., J. Phys. Oceanogr., 24, 466–497, 1194.

McManus, J., Francois, R., Gherardi, J.-M., Keigwin, L., and Brown-Leger, S.: Collapse and rapid resumption of Atlantic meridional circu-

25   lation linked to deglacial climate changes, Nature, 428, 834–837, 2004.

Meehl, G. A., Arblaster, J. M., Fasullo, J. T., Hu, A., and Trenberth, K. E.: Model-based evidence of deep-ocean heat uptake during surface-temperature hiatus periods, Nature Climate Change, 1, 360–364, 2011.

Melles, M., Brigham-Grette, J., Minyuk, P. S., Nowaczyk, N. R., Wennrich, V., DeConto, R. M., Anderson, P. M., Andreev, A. A., Coletti, A., Cook, T. L., Haltia-Hovi, E., Kukkonen, M., Lozhkin, A. V., Rosen, P., Tarasov, P., Vogel, H., and Wagner, B.: 2.8

30   Million Years of Arctic Climate Change from Lake El-gygytgyn, NE Russia, Science, 337, 315–320, doi:10.1126/science.1222135, http://www.sciencemag.org/content/337/6092/315.abstract, 2012.

Naish, T., Powell, R., Levy, R., Wilson, G., Scherer, R., Talarico, F., Krissek, L., Niessen, F., Pompilio, M., Wilson, T., Carter, L., DeConto, R., Huybers, P., McKay, R., Pollard, D., Ross, J., Winter, D., Barrett, P., Browne, G., Cody, R., Cowan, E., Crampton, J., Dunbar, G., Dunbar, N., Florindo, F., Gebhardt, C., Graham, I., Hannah, M., Hansaraj, D., Harwood, D., Helling, D., Henrys, S., Hinnov, L., Kuhn, G.,

35   Kyle, P., Lufer, A., Maffioli, P., Magens, D., Mandernack, K., McIntosh, W., Millan, C., Morin, R., Ohneiser, C., Paulsen, T., Persico, D., Raine, I., Reed, J., Riesselman, C., Sagnotti, L., Schmitt, D., Sjunneskog, C., Strong, P., Taviani, M., Vogel, S., Wilch, T., and Williams, T.: Obliquity-paced Pliocene West Antarctic ice sheet oscillations, Nature, 458, 322–328, 2009.

Park, W., Keenlyside, N., Latif, M., Ströh, A., Redler, R., Roeckner, E., and Madec, G.: Tropical Pacific climate and its response to global warming in the Kiel climate model., Journal of Climate, 22, 71–92, http://eprints.soton.ac.uk/64320/, 2009.

Peltier, W. and Solheim, L.: The climate of the Earth at Last Glacial Maximum: statistical equilibrium state and a mode of internal variability, Quaternary Science Reviews, pp. 335–357, 2004.

Philander, S., Holton, J., and Dmowska, R.: El Nino, La Nina, and the Southern Oscillation, International Geophysics, Elsevier Science, https://books.google.com/books?id=9fwrkW_B1YYC, 1989.

Pollard, D. and DeConto, R.: Modelling West Antarctic ice sheet growth and collapse through the past five million years, Nature, http://dx.doi.org/10.1038/nature07809, 2009.

Rayner, N. A., Parker, D. E., Horton, E. B., Folland, C. K., Alexander, L. V., Rowell, D. P., Kent, E. C., and Kaplan, A.: Global analyses of sea surface temperature, sea ice, and night marine air temperature since the late nineteenth century, Journal of Geophysical Research: Atmospheres, 108, n/a–n/a, doi:10.1029/2002JD002670, http://dx.doi.org/10.1029/2002JD002670, 4407, 2003.

Reynolds, R. W., Rayner, N. A., Smith, T. M., Stokes, D. C., and Wang, W.: An improved in situ and satellite SST analysis for climate, Journal of climate, 15, 1609–1625, 2002.

Scherer, R. P., Bohaty, S. M., Dunbar, R. B., Esper, O., Flores, J.-A., Gersonde, R., Harwood, D. M., Roberts, A. P., and Taviani, M.: Antarctic records of precession-paced insolation-driven warming during early Pleistocene Marine Isotope Stage 31, Geophysical Research Letters, 35, doi:10.1029/2007GL032254, http://dx.doi.org/10.1029/2007GL032254, 2008.

Schmitt, R., Bogden, P., and Dorman, C.: Evaporation minus precipitation and density flux for the North Atlantic, J. Phys. Oceanogr., pp. 1208–1221, 1989.

Severijns, C. A. and Hazeleger, W.: The efficient global primitive equation climate model SPEEDO V2.0, Geosci. Model Dev., 3, 105–122, doi:10.5194/gmd-3-105-2010, 2010.

Speer, K. and Tziperman, E.: Rates of water mass formation in the North Atlantic Ocean, J. Phys. Oceanogr., 22, 94–104, 1992.

Stocker, T. F., Dahe, Q., and Plattner, G.-K.: Climate Change 2013: The Physical Science Basis, Working Group I Contribution to the Fifth Assessment Report of the Intergovernmental Panel on Climate Change. Summary for Policymakers (IPCC, 2013), 2013.

Talley, D.: Shallow, intermediate, and deep overturning components of the global heat budget, J. Phys. Oceanogr., 35, 530–560, 2003.

Talley, D., Reid, L., and Robbins, E.: Data-Based Meridional Overturning Streamfunctions for the Global Ocean, J. Climate, 16, 3213–3226, 2003.

Teitler, L., Florindo, F., Warnke, D. A., Filippelli, G. M., Kupp, G., and Taylor, B.: Antarctic Ice Sheet response to a long warm interval across Marine Isotope Stage 31: A cross-latitudinal study of iceberg-rafted debris, Earth and Planetary Science Letters, 409, 109–119, doi:10.1016/j.epsl.2014.10.037, 2015.

Valcke, S.: The OASIS3 coupler: a European climate modelling community software, Geoscientific Model Development, 6, 373–388, doi:10.5194/gmd-6-373-2013, http://www.geosci-model-dev.net/6/373/2013/, 2013.

Villa, G., Lupi, C., Cobianchi, M., Florindo, F., and Pekar, S.: A Pleistocene warming event at 1Ma in Prydz Bay, East Antarctica: Evidence from ODP Site 1165, Palaeogeography, Palaeoclimatology, Palaeoecology, 260, 230 – 244, doi:http://dx.doi.org/10.1016/j.palaeo.2007.08.017, http://www.sciencedirect.com/science/article/pii/S0031018207005986, antarctic cryosphere and Southern Ocean climate evolution (Cenozoic-Holocene)1) {EGU} Meeting, 2) {XXIX} {SCAR} Meeting, 2008.

Voelker, A. H., Salgueiro, E., Rodrigues, T., Jimenez-Espejo, F. J., Bahr, A., Alberto, A., Loureiro, I., Padilha, M., Rebotim, A., and Rohl, U.: Mediterranean Outflow and surface water variability off southern Portugal during the early Pleistocene: A snapshot at Marine Isotope

Stages 29 to 34 (1020-1135 ka) , Global and Planetary Change, 133, 223 – 237, doi:http://dx.doi.org/10.1016/j.gloplacha.2015.08.015, 2015.

Wang, C., Weisberg, R. H., and Yang, H.: Effects of the wind speed-evaporation-SST feedback on the El Niño-Southern Oscillation, Journal of the atmospheric sciences, 56, 1391–1403, 1999.

5   Woodruff, S. D., Worley, S. J., Lubker, S. J., Ji, Z., Eric Freeman, J., Berry, D. I., Brohan, P., Kent, E. C., Reynolds, R. W., Smith, S. R., and Wilkinson, C.: ICOADS Release 2.5: extensions and enhancements to the surface marine meteorological archive, International Journal of Climatology, 31, 951–967, doi:10.1002/joc.2103, http://dx.doi.org/10.1002/joc.2103, 2011.

Yin, Q.: Insolation-induced mid-Brunhes transition in Southern Ocean ventilation and deep-ocean temperature, Nature, 494, 222–225, doi:10.1038/nature11790, 2013.

10   Yin, Q. Z. and Berger, A.: Individual contribution of insolation and CO_2 to the interglacial climates of the past 800000 years, Climate Dynamics, 38, 709–724, doi:10.1007/s00382-011-1013-5, http://dx.doi.org/10.1007/s00382-011-1013-5, 2012.

Zhang, Y., Wallace, J. M., and Battisti, D. S.: 1997: Enso-like interdecadal variability: 1900-93, Journal of Climate, 10, 1004–1020, doi:10.1175/1520-0442, 1997.
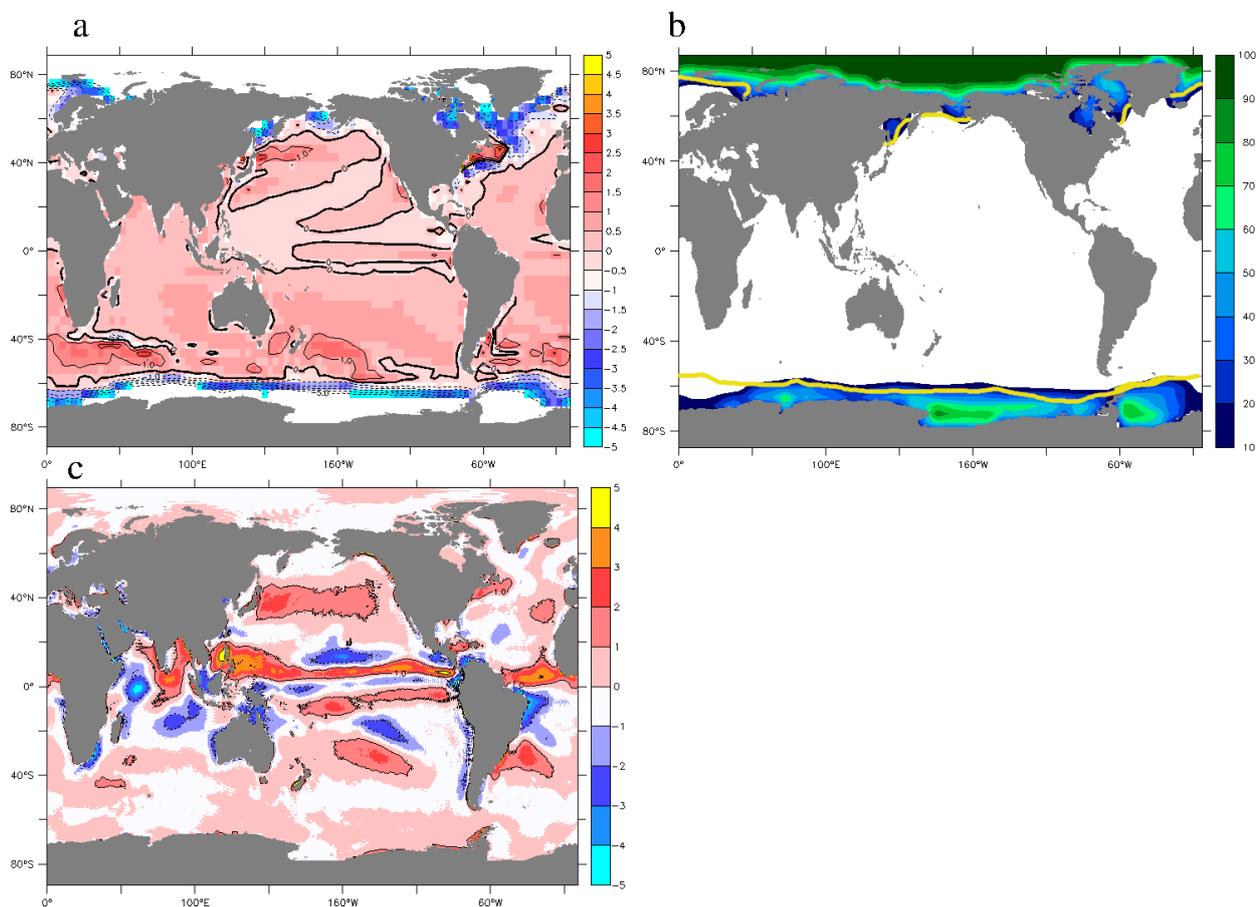
Figure 1. (a) Time-averaged surface temperature differences (°C) between the CTR and the NOAA-OI-surface temperature-V2 . The white shading indicates surface temperatures below -1.8°C. (b) Sea-ice cover based on the CTR (shaded in %) and the sea ice margin (yellow line) based on HadISST. (c) Time-averaged E - P flux differences (mm day^{-1}) between the control simulation and the ERAI.
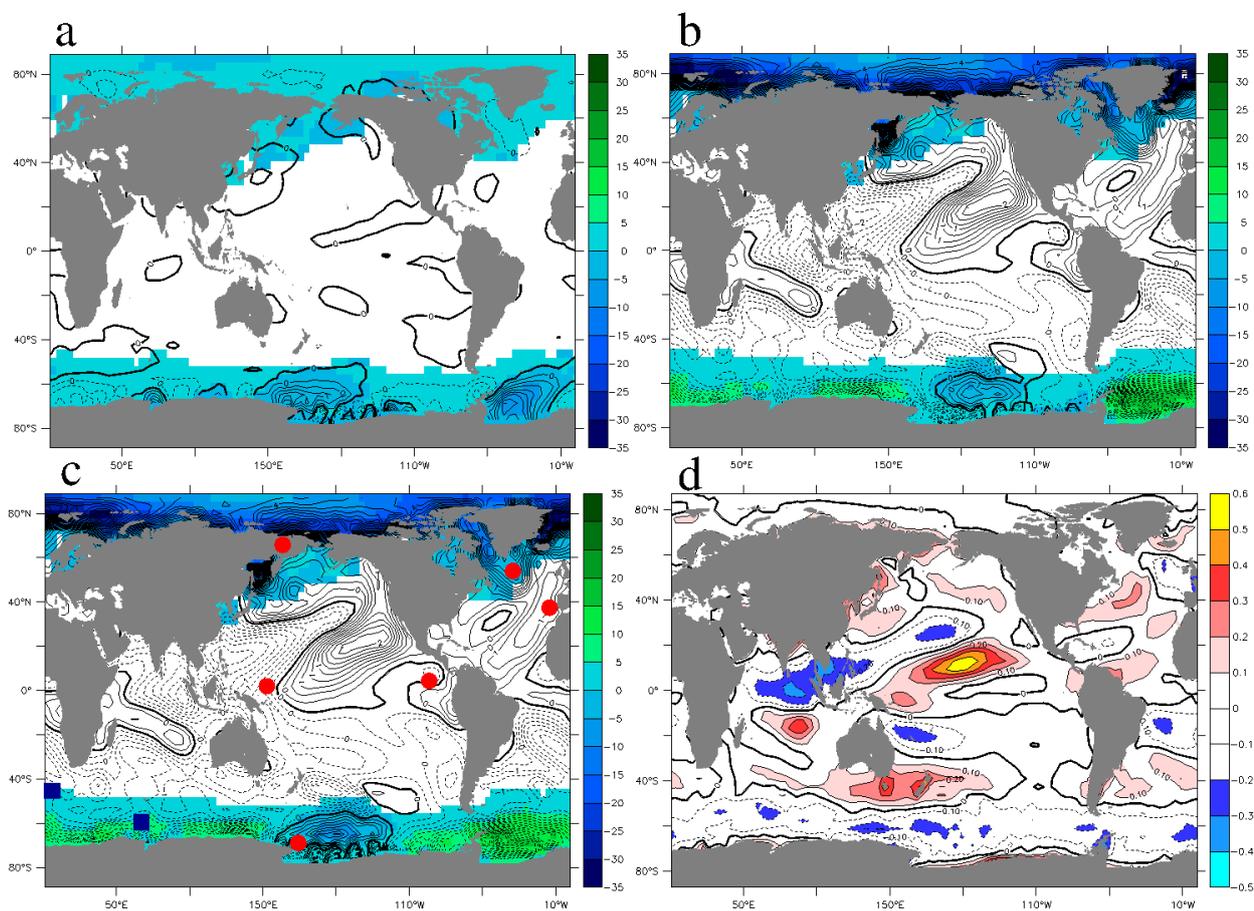
Figure 2. Time-averaged surface temperature differences (contour 0.2 interval, °C) between (a) TOPO, (b) AST, and (c) MIS31 compared to the CTR. Sea-ice cover differences (%) between the runs are shaded. (d) Wind-stress differences (10 x N m^{-2}) between the MIS31 and CTR. Land-ocean reconstructions are shown as red dots (warmer MIS31 conditions) and blue squares (colder MIS31 conditions).
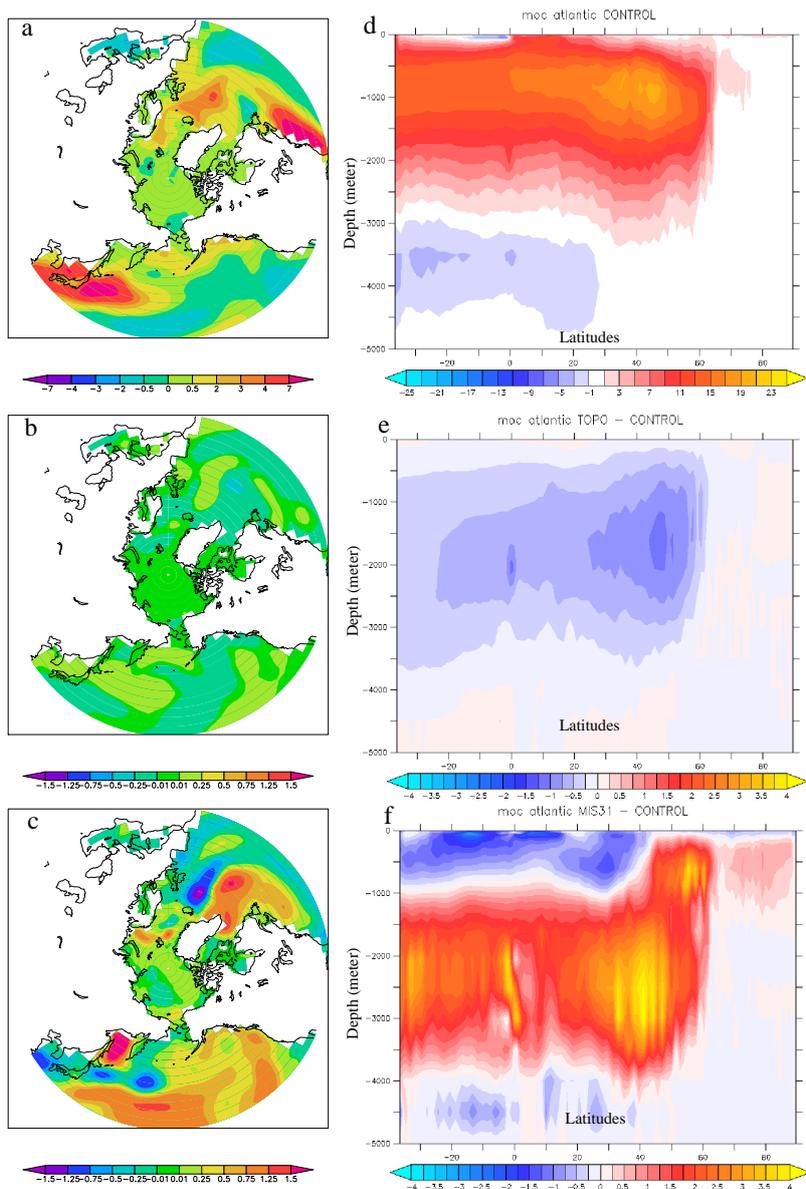
Figure 3. Density flux for CTR (a, 10^{-6} kg m^{-2} s^{-1}) and differences between the sensitivity experiments and CTR (b) TOPO, (c) MIS31.
(d) Time-averaged MOC (Sv) in the CTR and differences between the CTR and (e) TOPO and (f) MIS31.
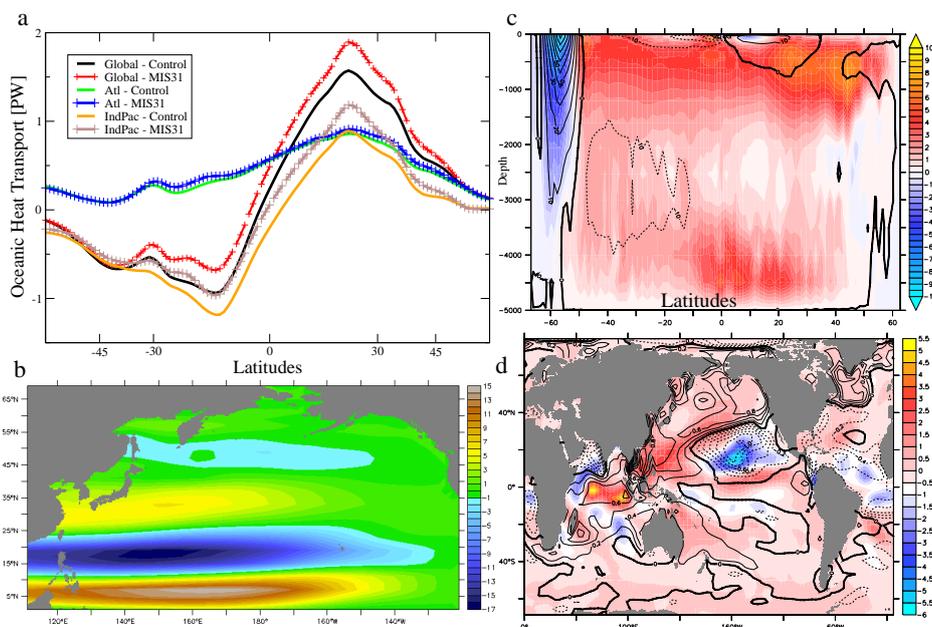
Figure 4. (a) Time-avaraged OHT (PW) for CTR (solid line) and MIS31 (dashed-crossed line). (b) Time-averaged Sverdrup transport differences (Sv) between the MIS31 and CTR. (c) Differences between the MIS31 and CTR MOC in the Pacific ocean (shaded, Sv), and contour shows the Pacific MOC in CTR. (d) E-P differences between CTR and MIS31 (shaded, mm day−1) and contours show differences in surface salinity between CTR and MIS31.
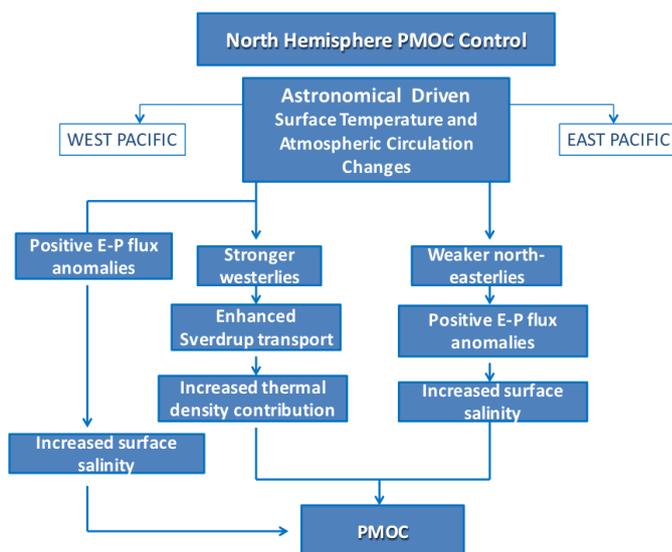
Figure 5. Flowchart showing the air-sea interaction mechanisms which are involved in the PMOC formation.

Table 1. Sea-ice volume (10^9 m^3) and area (10^9 m^2) in the NH and SH for CTR and sensitivity experiments.

	NH		SH	
	Volume	Area	Volume	Area
CTR	26439.5	10005.2	5016.9	8621.2
TOPO	26768.9	10076.6	4890.0	8611.7
AST	4412.1	7367.1	7641.4	10024.5
MIS31	4584.3	7456.7	7644.8	10203.1